X-622-71-272
PREPRINT

THE NIMBUS 4 INFRARED SPECTROSCOPY EXPERIMENT, IRIS-D

PART I
CALIBRATED THERMAL EMISSION SPECTRA

R. A. HANEL
B. J. CONRATH
V. G. KUNDE
C. PRABHAKARA
I. REVAH
V. V. SALOMONSON
G. WOLFORD

JULY 1971

GSFC
GODDARD SPACE FLIGHT CENTER
GREENBELT, MARYLAND

X-622-71-272
PREPRINT

THE NIMBUS 4 INFRARED SPECTROSCOPY EXPERIMENT, IRIS-D

PART 1
CALIBRATED THERMAL EMISSION SPECTRA

by

R. A. Hanel, B. J. Conrath, V. G. Kunde, C. Prabhakara,
I. Revah, V. V. Salomonson, and G. Wolford

July 1971

GODDARD SPACE FLIGHT CENTER
Greenbelt, Maryland

THE NIMBUS 4 INFRARED SPECTROSCOPY EXPERIMENT, IRIS-D

PART I
CALIBRATED THERMAL EMISSION SPECTRA

R. A. Hanel, B. J. Conrath, V. G. Kunde, C. Prabhakara,
I. Revah, V. V. Salomonson, and G. Wolford

ABSTRACT

The infrared interferometer spectrometer carried on the Nimbus 4 meteorological satellite measures the infrared spectrum of the earth and atmosphere between 400 and 1600 cm^{-1}. The instrument is similar to one flown on Nimbus 3, but a number of improvements have been implemented, including higher spectral resolution (2.8 cm^{-1}), higher spatial resolution (5 degree field of view), and a lower noise equivalent radiance (0.5 to 1.0 $erg\text{-}s^{-1}\text{-}cm^{-2}\text{-}ster^{-1}/cm^{-1}$). In an effort to obtain spectra with high absolute accuracy, it was necessary to incorporate many factors into the calibration, including small departures from unity in the emissivity of the onboard calibration source, imbalance between cold and warm calibration ports, and effects due to orbital variations in instrument temperature. The inclusion of such higher order corrections, along with careful data screening processes, has insured a high quality data set which can be used in a variety of geophysical and

meteorological investigations. This set is available to qualified investigators. Representative samples of data are presented which illustrate the behaviour of the thermal emission spectra under a variety of conditions encountered in a typical orbit, including extremes in temperature, surface reststrahlen effects, and various types of cloud conditions. The data are being used currently in a number of investigations which include a study of radiative transfer processes in the atmosphere, examinations of vertical sounding techniques, studies of the statistical properties of the spectra, and the study of global fields of temperature and ozone.

CONTENTS

	Page
ABSTRACT	iii
INTRODUCTION	1
INSTRUMENT	5
FOURIER TRANSFORMATION AND QUALITY CONTROL	8
PHASE CORRECTION	10
CALIBRATION	11
EMISSIVITY CORRECTION	14
SPECTRAL CORRECTION	14
ORBITAL TEMPERATURE CORRECTION	17
RESPONSIVITY AND NOISE EQUIVALENT RADIANCE	19
IMAGE MOTION COMPENSATION	20
DATA FORMAT OF USER'S TAPES	22
CALIBRATED SPECTRA	23
PLANNED INVESTIGATIONS	27
ACKNOWLEDGMENT	28
REFERENCES	29
FIGURE CAPTIONS	31

THE NIMBUS 4 INFRARED SPECTROSCOPY EXPERIMENT, IRIS-D

PART 1
CALIBRATED THERMAL EMISSION SPECTRA

by

R. A. Hanel, B. J. Conrath, V. G. Kunde, C. Prabhakara,
I. Revah*, V. V. Salomonson, and G. Wolford
Goddard Space Flight Center

INTRODUCTION

Until the launch of Nimbus 3 in April 1969, the main thrust of the United States meteorological satellite program had been the use of imaging systems to register the global distribution of clouds on a variety of spatial and temporal scales. Television cameras and scanning infrared radiometers were the main tools of meteorological research and the only devices used operationally. Before the launch of Nimbus 3, some satellite-borne instruments generated data for studies of the heat balance of the earth and for other tasks in atmospheric physics (Möller and Raschke, 1969), but it was not until Nimbus 3 that a major step was taken beyond the recording of the state of cloudiness. The satellite infrared spectrometer (SIRS) (Wark and Hilleary, 1969) and the infrared interferometric spectrometer (IRIS) (Hanel and Conrath, 1969) aboard Nimbus 3 have opened literally a new dimension of atmospheric research from space. Both experiment systems yielded vertical temperature profiles, and IRIS yielded water vapor and ozone profiles as well.

*NAS/NRC Resident Research Associate. Present address: Centre Nationale d'Etudes des Telecommunications, Paris, France.

Nimbus 4, launched in April 1970, carries improved versions of both instruments and a third instrument for remote atmospheric temperature measurements, the selective chopper radiometer (SCR) developed by Houghton and Smith (Ellis et al., 1970). All these devices derive atmospheric temperatures from measurements of the infrared radiance in relatively narrow spectral intervals in the 667 cm^{-1} (15μm) band of CO_2. The small amount of energy available in these narrow intervals and the high precision required to derive useful profiles were the main challenges in the development of these instruments and the reasons why these measurements were not performed much earlier. The basic principles of vertical sounding of atmospheric temperatures have been known for more than a decade (Kaplan, 1959; King, 1956).

SIRS and SCR were designed for a very specific task, the remote measurement of atmospheric temperature; on Nimbus 4, SIRS was used to measure humidity also. For these specific goals, it is sufficient to record the radiance in a relatively small number of intervals correctly chosen in the infrared spectrum. In this sense, SIRS and SCR are multichannel radiometers, in contrast to IRIS which functions as a spectrometer and records a large and continuous portion of the thermal emission spectrum, including intervals suitable for vertical temperature analysis. Consequently, the IRIS data reduction is much more complex than that for instruments devoted only to vertical sounding. However, a larger number of research goals can be pursued with the continuous spectra than can be pursued with a small number of radiance measurements.

The derivations of the vertical profiles of temperature, humidity, and ozone are certainly important aspects of the IRIS experiment, but IRIS is broader in scope, as will be apparent from the following discussions.

The basic theory of remotely sensing atmospheric and surface parameters by interpretation of the thermal emission spectrum is well established for a clear atmosphere in local thermodynamic equilibrium (LTE). The fundamentals are discussed for example, in a paper on the results obtained with the Nimbus 3 interferometer (Conrath et al., 1970). However, two aspects of the IRIS experiments on Nimbus 3 and 4 must be emphasized: a wide spectral range and a relatively high spectral resolution. For the task of mapping the three-dimensional temperature field for operational meteorological purposes, neither one is of fundamental importance. For the operational task of temperature probing, a rather limited number of spectral intervals, about 10, seems to be adequate, and little is gained by the addition of one or more channels since they would largely provide redundant information. Further, in the 667 cm^{-1} CO_2 band, a spectral resolution of 5 to 20 cm^{-1} seems to be sufficient if analysis of the first 25 or 30 km of the atmosphere is sought. For the operational system, high radiometric precision, moderate spatial resolution, and, above all, good global coverage are more important than wide spectral coverage and high spectral resolution.

The research requirements in this field are different, however. For many research purposes, the optimum frequency intervals which carry the

significant information cannot be specified precisely in advance. Experimental results are needed to advance the theoretical treatment of radiative transfer calculations under non-LTE conditions in the real atmosphere. The selection of the optimum spectral range and resolution for operational systems, analyses of radiative transfer in the presence of haze and clouds, the search for and the tracing of minor gaseous constituents, and many other tasks to be discussed later in this series of papers are performed best with continuous spectra of high spectral resolution. It was from these research-oriented considerations that the IRIS parameters were chosen.

The purpose of this series of papers is to present the scientific results of the Nimbus 4 interferometer experiment. The variety of research tasks which may be pursued with the Nimbus 4 infrared spectra is too large to be treated adequately in a single publication. Therefore, a series of papers is in preparation, each one being devoted to a specific topic. However, even after completion of these papers, only a fraction of possible research tasks will have been accomplished. Other researchers may use this unique set of spectra for a variety of individual goals, some of which may not be visualized fully even now. Interested researchers may obtain the calibrated IRIS spectra from the National Space Science Data Center.* To familiarize a potential user with the data and to permit a judgment of the quality of the spectra, the first paper in

*National Space Science Data Center, Code 601, Goddard Space Flight Center, Greenbelt, Maryland 20771.

this series is devoted to an overview of the experiment and to a discussion of the data processing techniques applied to yield calibrated spectra which will serve as the point of departure for all further investigations. A user of IRIS data should be familiar with the reduction procedures and be aware of potential problems associated with the handling of large quantities of real data.

Subsequent papers will start with the calibrated spectra in pursuit of specific research investigations, such as studies of problems in radiative transfer and atmospheric transmittances, the derivation of atmospheric temperatures, humidities, and ozone concentrations, spectral correlation analyses and other statistical information processing, and several tasks of a meteorological nature.

INSTRUMENT

The Nimbus 4 infrared spectrometer, IRIS -D, is a single detector Michelson interferometer. The design and performance of this instrument have been discussed elsewhere (Hanel et al., 1971). Here, it is sufficient to summarize the basic properties of the instrument and the concentrate on the orbital performance of the interferometer as far as it may be of interest to a user of the data.

The instrument is an improved version of IRIS-B flown a year earlier on Nimbus 3 (Hanel et al., 1970). Signals from the detector, the interferograms, are Fourier transformed into spectra and then subjected to a calibration procedure in a ground-based digital computer. Spectra of the earth are being obtained between 400 cm^{-1} (25μm) and 1600 cm^{-1} (6.3μm) with a

nominal spectral resolution of 2.8 cm^{-1}. In comparison, IRIS-B had a resolution of 5 cm^{-1}.

The noise equivalent radiance (NER) of IRIS-D is estimated to be between 0.5 and 1.0 $erg\text{-}s^{-1} - cm^{-2} - ster^{-1}/cm^{-1}$* over most of the spectral range but is slightly higher at both ends of the range. Originally, IRIS-B had a NER of about the same level, but the NER increased shortly after orbit insertion by about 30 percent at the low wave number end of the spectrum and by more at the high end. The NER of IRIS-D has not changed significantly in orbit and has consistently been better then the NER of IRIS-B.

The field of view of IRIS-D is a cone of 2.5 degree half angle, somewhat smaller than the 4 degree of IRIS-B. An area of about 95 km diameter is observed from the Nimbus 4 altitude during the 13 seconds it takes to record one interferogram. Image motion compensation is applied to minimize target smear. The three second gap between interferograms is used to return the Michelson mirror and the image motion compensator to the start position. In 16 seconds, the time between starts of successive interferograms, Nimbus moves approximately 110 km so that the observed areas form an almost contiguous pattern along the subsatellite path. Every 15th and 16th interferogram is taken while observing the built-in warm blackbody and outer space, respectively, for calibration purposes. Approximately 400 interferograms are

* 1 $erg\text{-}s^{-1} - cm^{-2} - ster^{-1}/cm^{-1}$ equals 10^{-7} $watt\text{-}cm^{-2} - ster^{-1}/cm^{-1}$

recorded per orbit and in the average about 4000 per day, which amounts to more than one million spectra per year.

The main differences between IRIS-B and D are a higher spectral resolution, a narrower field of view, and a somewhat lower NER for the latter model. Improvements in the servo systems and main infrared data channel are primarily responsible for the better performance of IRIS-D compared to that of its predecessor. Otherwise, the interferometers on Nimbus 3 and 4 are very much alike. For example, the beam splitter of IRIS-D is similar to the potassium bromide beam splitter of IRIS-B, and a thermistor bolometer serves in both instruments as the infrared detector.

The interferometer on Nimbus 4 operates at a temperature of about 250K, sometimes within the range of the thermostat but more often just 1 or 2K above. As a consequence, the instrument undergoes small temperature changes in synchronism with the orbital position of Nimbus. The effect of these temperature changes is small but not negligible, and its removal will be discussed later. Corrections will be applied also to compensate for the nonblackness of the warm calibration "blackbody" and for differences in the responsivities between the earth port and the cold calibration port. Another slight imperfection in the instrument performance developed gradually after several months in orbit. Beginning about September 1970, some increase in the friction of the torque motor used in the image motion compensation circuit caused a small amount of smear of the field of view. The effect of the smear will be discussed also.

Except for the areas just mentioned, which are all of minor consequence as far as the quality of the spectra is concerned, the interferometer performed close to the theoretically possible limits. Continuous operation over a long period of time is being achieved without a noticeable degradation of the instrument performance. As of this writing, a full year of operation has been logged.

FOURIER TRANSFORMATION AND QUALITY CONTROL

The first step in the data reduction process, the Fourier transformation of the interferograms into raw power and phase spectra by the Cooley-Tukey algorithm takes 0.9 seconds for each interferogram of 4096 words on the IBM 360-91 computer. An apodisation function (Hanel et al., 1970) is applied to all interferograms. Because of the active control of the interferogram start position of the Michelson mirror, the center word within an interferogram is repeatable enough to avoid a shift of the zero-phase reference point as was sometimes required in the IRIS-B data reduction (Hanel et al., 1970).

Experience with IRIS-B has shown also the need for better error rejection at this stage of data reduction. The bit error rate of the Nimbus telemetry system is low, much less than one error in 10^5 bits, but the long chain of events between the recording of the signal in the satellite and the processing in the ground-based computer is not free of occasional errors. If they were not recognized and corrected, spectra with serious defects would occur every orbit. An experienced investigator can recognize certain defects in the display, but visual inspection of all spectra is prohibited by the large

quantities involved. An attempt was made to design several error detection, correction, and, if necessary, rejection criteria into the computer processing to reduce the probability that erroneous spectra enter the final data record. The interferograms are subjected to screening procedures, slightly different for those from atmospheric observations than for those from the warm and cold calibration targets. The amplitudes of all interferogram words must fall within prescribed boundaries (see Figure 1). Individual bit errors often cause a large amplitude in a particular word, which can be recognized as a spike in the interferogram. The computer program automatically replaces the bad interferogram word with a new one derived from an 11th-order interpolation. It was shown by simulation that the error in the spectrum which results from this procedure is smaller than the NER, and, therefore, it is considered acceptable. The same procedure is applied to as many as three spikes, each one up to three words wide, provided the spikes are not too close to each other to prevent interpolation; otherwise, the whole interferogram is rejected.

Calibration interferograms are subjected to an additional test. The strong central peak of the calibration interferograms must fall within five words of the predicted word number and within about 10 percent of the predicted positive or negative amplitude, respectively; otherwise, the particular interferogram is rejected. This procedure is designed to make it unlikely that atmospheric spectra enter the ensemble of calibration spectra.

Another correction is applied to all calibration interferograms. Whenever the general radiation background on the detector changes drastically, a transient occurs which did not decay completely until about word number 150 of the next interferogram. This transient was observed in the interferograms from the warm blackbody, which follow those from the cold calibration. The first and last 150 words are therefore ignored in all calibration interferograms. The resulting slightly lower spectral resolution (by 7 percent) of the calibration spectra is insignificant.

The housekeeping measurements also are subjected to several error correction procedures. For example, the warm blackbody temperature is measured four times before and four times after each interferogram. If one of these measurements deviates by more than 5K from the expected value, it is rejected. At least four of the eight readings must be available for averaging to constitute a valid temperature measurement in the housekeeping channels.

From the first month of available data, about 1.2 percent of all interferograms were rejected by the quality control tests. Then, the screened interferograms are Fourier transformed into amplitude and phase spectra as mentioned earlier.

PHASE CORRECTION

The next step in the data reduction process is the phase correction. The operation of IRIS at the midrange of expected brightness temperatures requires the use of the phase spectrum to resolve the ambiguity between scenes warmer

or colder than the instrument. The general procedure discussed previously (Hanel et al., 1970) was used again, except that the averaging of the phase curve which represents the phase colder than the instrument was carried out over 140 wave numbers instead of over 40 wave numbers as was done previously. A somewhat smoother phase reference curve resulted, particularly noticeable close to the 1600 cm^{-1} limit.

At this point in the data processing, another quality control check is made. The mean slope of the phase spectrum between 640 and 680 cm^{-1} must be less than a given limit. This is equivalent to requiring the central peak of the calibration interferograms to lie within 5 words of the predicted value, but the phase slope criterion applies also to atmospheric spectra which may not have a central peak in their interferograms. In the 640 to 680 cm^{-1} interval, the brightness temperature of the earth is always below the instrument temperature, and, therefore, 180 degree phase transitions are not expected in this interval. Then, the amplitude of the phase-corrected raw power spectrum is subjected to the calibration procedure.

CALIBRATION

In the preliminary calibration procedure, the radiance of the scene is determined by scaling the raw atmospheric spectra to the calibration spectra; this is described by Hanel et al., (1971). All Nimbus 4 spectra published to date have been computed in this way. The final data reduction process, however, applies several refinements which correct for deviations from ideal

blackness of the warm reference, for an imbalance of the deep space calibration, and finally for the dependence of some parameters on the satellite position with respect to the earth's shadow. Therefore, the basic calibration equations are reformulated considering radiative energy exchange between three surfaces; this is shown in Figure 2.

The radiant power P_{out} emerging from surface A_1 which has emissivity ϵ_1, within the solid angle Ω_1 (all solid angles are normalized to the hemisphere) consists of an emission and a reflection term (reflectivity equals $1-\epsilon_1$):

$$P_{out} = \epsilon_1 B_1 + (1-\epsilon_1)\, P_{in} . \qquad (1)$$

The radiance of a black emitter (Planck function) is denoted by $B(\nu, T)$. The incoming power, again within Ω_1 of A_1, may be expressed as the emitted radiance from A_2 plus radiation reflected from that surface. The power falling on A_2 is considered to originate from A_1 within Ω_2 and otherwise from A_3, which is assumed to have unit emissivity:

$$P_{in} = \epsilon_2 B_2 + (1-\epsilon_2)\left[P_{out}\,\Omega_2 + B_3\,(1-\epsilon_2)\right] . \qquad (2)$$

The net power is

$$\Delta P = P_{in} - P_{out}$$

$$= \frac{\left[(1-\epsilon_2)\,\Omega_2 - 1\right]\epsilon_1 B_1 + \epsilon_1\epsilon_2\, B_2 + \epsilon_1(1-\epsilon_2)(1-\Omega_2)\, B_3}{1-(1-\epsilon_1)(1-\epsilon_2)\,\Omega_2} . \qquad (3)$$

In the following, A_1 and Ω_1 are identified with the aperture and field-of-view of the interferometer. A_2 represents the earth, deep space, or the warm calibration blackbody, depending on the position of the calibration mirror. A_3 represents either deep space or the internal cavity of the instrument.

The net power for the earth view (target), cold calibration, and warm calibration, respectively, is

$$\begin{aligned} \Delta P_t &= \epsilon_i (I_t - B_i), \\ \Delta P_c &= -\epsilon_i B_i, \\ \Delta P_w &= \epsilon_i \epsilon_w (B_w - B_i), \end{aligned} \tag{4}$$

where $\epsilon_2 B_2$ of Equation 3 is called I_t, the unknown radiance of the earth. Some terms were neglected since Ω_2, even for the warm calibration blackbody, is very small, of the order of 10^{-3} or smaller. The spectral amplitudes C measured by the interferometer are proportional to the net power and is given for the same three cases by

$$\begin{aligned} C_t &= r(I_t - B_i), \\ \beta C_c &= r B_i, \\ \alpha C_w &= r(B_w - B_i), \end{aligned} \tag{5}$$

respectively. The proportionality factor r is called the responsivity, which includes the emissivity of the interferometer ϵ_i. The factor α represents the reciprocal value of the emissivity of the warm blackbody, and β is used to

account for the unbalance of the cold calibration port. Both factors become unity under ideal conditions; in this case, Equation 5 is identical to the preliminary calibration equations given by Hanel et al. (1970).

EMISSIVITY CORRECTION

In the preliminary procedure, the warm calibration source built into the instrument has been assumed to be perfectly black. However, small deviations from ideal conditions are to be expected. The reflectivity of the grooved and blackened plate which serves as the warm calibration source was measured as a function of wave number. The results are shown somewhat smoothed in Figure 3. The warm calibration source is practically an ideal blackbody except for a feature near 1100 cm^{-1} which is attributed to minerals, probably SiO_2, in the black paint used. As mentioned before, the correction factor $\alpha(\nu)$ is the reciprocal value of the emissivity $\epsilon_w(\nu)$.

SPECTRAL CORRECTION

The basic calibration procedure chosen for IRIS, namely the exposure of the instrument to both warm and cold reference sources, is to some degree redundant – one knows a priori that when the interferometer is exposed to a blackbody of the same temperature the net flux from the interferometer is zero. This redundancy may be used to check the procedure and apply corrections, such as the β factor in Equation 5, if necessary. A particular check is the comparison of the instrument temperature calculated from the cold and warm calibration spectra with the temperature measured by thermistor elements

imbedded in the interferometer. In Figure 4, the calculated instrument temperature is somewhat lower than the thermistor value and, moreover, it deviates significantly from the expected horizontal line, particularly above 1200 cm^{-1}.

An investigation has shown that the amplitude of the cold calibration signal is slightly deficient. Errors in the blackbody or instrument temperature measurements can be ruled out. A number of possible explanations for this deficiency are identified, but so far a quantatively satisfying solution has not been found.

First, in the cold calibration position, the 45 degree mirror which exposes the instrument to the different calibration sources and to the earth is positioned at 90 degrees with respect to the earth port as well as to the warm blackbody direction. Polarization introduced by the 45 degree mirror could cause a difference in the responsivity for the cold and warm calibrations. Calculations using the appropriate form of Fresnel's equation and the complex refractive index for a gold surface at 45 degree show that this effect should be negligible. However, the same equation predicts for normal incidence a reflectivity of 0.998 at 2000 cm^{-1}, which is considerably higher than realistic experimental values.

Second, a small nonlinearity in the detector or in the analog portion of the infrared data channel may exist. A noticeable nonlinear effect on the electronic filter can be seen when the signal exceeds -6 V, which is one volt below the range of the analog-to-digital converter (+5 to -5 V). The cold blackbody

interferogram has an amplitude of about -4.6 V while the warm blackbody peak signal is only +3.5 V; therefore, an effect, if it should exist, would be expected to affect the cold more than the warm calibration.

Third, the light shield of the calibration port is longer than that of the earth port, and a very short shield is used on the warm blackbody. Stray radiation from the shield would affect the cold calibration port more than the others and may contribute in this way to the imbalance. The polarity of the effect is in the required direction, but the shape of the correction factor seems to disagree with this explanation.

Whatever the cause may be, possibly a combination of several effects, it is evident that a correction should be applied to the signal from the deep space port. From Equation 5, the factor β was calculated to be

$$\beta = \frac{\alpha C_w}{C_c} \cdot \frac{B_i}{B_w - B_i} \quad . \tag{6}$$

All parameters depend on ν. The temperature employed in the calculation of B_i is the average of the measurements from two thermistor elements located in the interferometer housing, one near the beam splitter and the other one near the bolometer mount. The average β, which is shown somewhat smoothed in Figure 5, was calculated from about 50 orbits uniformly distributed over the first four months of operation of Nimbus 4.

Without the β factor, the absolute calibration of IRIS is based on the warm blackbody and cold interstellar space. With the β factor applied, the

absolute scales are governed by the blackbody and the instrument temperature. This procedure may seem arbitrary, but it derives its justification from improvements in the absolute levels in the obtained spectra. For example, without the β factor, negative values occur quite often at the high wave number end of the spectrum, but most disappear after β is applied.

ORBITAL TEMPERATURE CORRECTION

As a consequence of changing solar illumination on the spacecraft, the interferometer undergoes small temperature variations, of the order of one or two degrees, synchronized with the orbital position ϕ of the satellite with respect to the earth's umbra. These temperature variations cause atmospheric, as well as calibration spectra to vary somewhat with orbital position. It would be completely adequate to use the particular cold and warm calibration pairs closest in time to an atmospheric spectrum; however, this is undesirable for two reasons. First, nearby calibration spectra are not always available; sometimes they are rejected for errors, or sometimes calibration is inhibited intentionally (for example, over the north polar regions to avoid sunlight falling onto the detector). Second, random noise in the calibration spectra enters a calibrated atmospheric spectrum strongly if only a single pair of a cold and a warm calibration spectrum is used. For these reasons, another approach was taken.

The spectral amplitude of a particular calibration may be considered to depend on the wave number ν, the orbital position of the satellite with respect to the umbra ϕ, and the orbit number i, which in turn depends on the day d.

Instead of the instantaneous value of the spectral amplitude $C(\nu, \phi, i)$, the daily averages $\bar{C}(\nu, d)$ are used, and the orbital position dependence is expressed by the factors $\Phi(\phi)$ and $\Psi(\phi)$ for the cold and warm calibration spectra, respectively. The functions Φ and Ψ have been calculated from mean values of C over ν and i, after it was established that the dependence of Φ and Ψ on ν and i was indeed negligible. Daily averages of Φ and Ψ displayed for the period April to August 1970 show no trend; secular changes of the instrument's sensitivity could not be detected. The deviations of Φ and Ψ from unity are small, less than 1.5 percent (see Figure 6), but nevertheless enough to be recognized.

The averaging of the calibration spectra on a daily basis instead of on an orbital basis, as with IRIS-B, provides a better signal-to-noise ratio in the calibration spectra, since more are averaged, and avoids problems which may arise when only a small fraction of an orbit with only a few calibrations is available.

The final equation used in the reduction of atmospheric spectra is

$$I(\nu, \phi, i) = \frac{C_t(\nu, \phi, i) - \beta(\nu)\Phi(\phi)\,\bar{C}_c(\nu, d)}{\alpha(\nu)\psi(\phi)\,\bar{C}_w(\nu, d) - \beta(\nu)\Phi(\phi)\,\bar{C}_c(\nu, d)} B\left[\nu, \bar{T}_w(\phi, i)\right]. \quad (7)$$

The temperature T_w of the warm blackbody also varies slightly with the orbital position. The readings from the platinum wire thermometer taken four times before and four times after each interferogram are very close to each other which shows there is no need for smoothing on an orbital scale. To smooth out small quantization steps, a local averaging $\bar{T}_w$ over 16 interferograms is performed in the computation of the Plank function of Equation 7.

RESPONSIVITY AND NOISE EQUIVALENT RADIANCE

The correction factors discussed above enter not only the equation used to calibrate the raw atmospheric spectra but also the equations of the responsivity and the noise equivalent radiance (NER). Consistent with the derivation of the correction factors, the instantaneous responsivity may be calculated from Equation 5,

$$r(\nu, \phi, i) = \frac{a(\nu) C_w(\nu, \phi, i) - \beta(\nu) C_c(\nu, \phi, i)}{B(\nu, \bar{T}_w(\phi, i))} \quad . \tag{8}$$

Three daily mean values of the responsivity $r(\nu, d)$ are displayed in Figure 7.

The NER is calculated from the standard deviation of the instantaneous responsivities derived from individual calibration pairs, $r(\nu, \phi, i)$, with the help of

$$NER(\nu, d) = \frac{s(r)\, B(\nu, \bar{\bar{T}}_w)}{\sqrt{2}\ \ \bar{r}(\nu, d)} \quad , \tag{9}$$

where $\overline{\overline{T}}_W$ represents the daily mean blackbody temperature (see Hanel et al., 1971, Equation 11). The sample standard deviation s(r), is computed not with respect to the daily mean values of the responsivity but with respect to the predicted values for a particular orbit position. In other words the deviations between the instantaneous responsivity, given in Equation 8, and value r_0, given by

$$r_0(\nu, \phi, i) = \frac{\alpha(\nu)\psi(\phi)\,\overline{C}_W(\nu, d) - \beta(\nu)\Phi(\phi)\,\overline{C}_c(\nu, d)}{B\left(\nu, \overline{T}_W(\phi, i)\right)} \quad , \qquad (10)$$

were used, which takes the systematic variation of r with respect to ϕ fully into account. With this procedure, the NER represents the repeatability of the measurement limited primarily by random effects. The systematic variations caused by the orbital temperature variations have been removed to the same degree as in the atmospheric spectra. Examples of the computed NER are shown in Figure 8 for three days within the first three months of data available.

IMAGE MOTION COMPENSATION

IRIS-D, as well as its predecessor IRIS-B, is designed to have image motion compensation. On IRIS-D, after several months in orbit, the amplitude of rotation of the 45 degree mirror gradually reduced to about 75 percent of its design value. This causes the field of view to move during the 13 seconds required to record an interferogram. While the instrument is viewing a homogeneous background, the effect of smear on the quality of the spectra

should be negligible, but this is not obvious for an inhomogeneous scene. The latter is more likely to occur in reality.

To investigate the effect of smear, two interferograms were chosen, A and B in Figure 9. The corresponding spectra are shown in Figure 10. Interferogram "A" represents a very cold cloud which fills the field of view completely; interferogram B is a cloud-free case over tropical water taken not far apart from interferogram A. Interferograms A and B are averaged in two ways. First, an average interferogram is computed, not shown in Figure 9, and transformed to give spectrum (A+B)/2 of Figure 10. This spectrum corresponds to the case when one half of the field of view is clear and the other half is covered with dense, high clouds. It simulates the case of an extremely inhomogeneous background observed with perfect image motion compensation. Second, the same interferograms A and B are combined to simulate a complete lack of image motion compensation. At the beginning of interferogram C, only A contributes, the effect of interferogram B gradually increases, and toward the end, interferogram B dominates. This represents a situation where, at the beginning, the instrument would view a homogeneous cold cloud, then would scan gradually across the sharp boundary, and would terminate the interferogram just when the cloud had passed out of the field of view completely, and only the warm ocean was observed. The calculations assume a circular field of view.

The resulting spectrum, C in Figure 10, is not distinguishable from the linear average (A+B)/2 in the graphical display. An examination of the

numerical values shows that the difference between the spectra is of the order of 0.1 erg-s^{-1} - cm^{-2} - ster^{-1}/cm^{-1} and, even in the unapodized mode of data reduction, rarely approaches 0.5 erg-s^{-1} - cm^{-2} - ster^{-1}/ cm^{-1}. Since this is smaller than the NER and since the case analyzed is much more severe than the 25 percent reduction in image motion actually experienced, it is concluded that the quality of the spectra has not suffered at all, and, therefore, corrective steps in the data reduction to compensate for smear are not required. The only effect which may have to be considered in the interpretation is the slight elongation of the effective field-of-view. During the first months in orbit, the field of view of IRIS-D covered a circle 95 km in diameter on the earth's surface, but later, the effective field increased in the direction of the satellite motion to cover an area about 95 by 120 km.

This concludes the discussion of the calibration procedure and of the correction terms that were applied to the raw data. A considerable effort had to be devoted to preparing the computer programs to carry out these tasks automatically, and sample spectra from every orbit were inspected visually. Only in this way is it possible to process the large quantity of spectra. To date, only the first three months of raw data have been processed, but it is hoped that a full year of calibrated spectra will be available eventually.

DATA FORMAT OF USER'S TAPES

As mentioned before, the calibrated IRIS spectra are available from the Space Science Data Center. On request, copies will be made from archival

magnetic tapes which have 9 tracks and a 1600 bit per inch packing density. The tapes contain a single file composed of variable format records written by FORTRAN IV unformatted WRITE statements on the IBM Operating System 360. Each record contains data in 16 binary bit and 32 binary bit integer format and IBM 360 single-precision floating point format. Each tape contains data for a period of approximately 24 hours beginning and ending at about midnight GMT. The first seven records on each tape are statistical data accumulated over a day. The first record contains the daily means and rms deviations of the temperatures of various components of the IRIS instrument and a list of the contiguous time segments of the data on the tape. The second and third records contain, respectively, the daily mean cold and warm calibration spectra. The fourth through the seventh records contain, respectively, the responsivity, the NER, the instrument temperature, and the rms deviation of the instrument temperature, each computed from contiguous cold and warm calibration spectra. The remaining records are individual calibrated spectra of the earth for that 24 hour period; each spectrum is identified by a time code.

Further details on the format and content of the magnetic tape are contained in a user's guide book which is available with the tapes.

Calibrated Spectra

Subsequent papers of this series will present more comprehensive analyses, but Part 1 would be incomplete without representative samples of

spectra recorded in orbit. In Figures 11 through 14, the spectral radiance of the terrestrial emission, together with the Planck function for several temperatures, is plotted as a function of wave number.

The spectra that are shown in Figure 11 were recorded over West Africa during orbit 365 on May 5, 1970. The maximum brightness temperature measured in the "atmospheric windows" between 850 and 950 cm^{-1} indicates surface temperatures in excess of 320 K. If residual atmospheric absorption is ignored, this temperature refers to the top layer, perhaps a few micrometers thick, of exposed soil or vegetation. At local noon, this surface is expected to be warmer than the air measured, for example, in a meteorological shelter (Buettner and Kern, 1965).

The hot surface contrasts sharply with the absorption features of gases in the cooler atmosphere. Between approximately 600 and 750 cm^{-1}, the spectrum is dominated by carbon dioxide absorption and reemission; ozone is responsible for the shape of the curves between 1000 and 1070 cm^{-1}. Most of the other features are caused by water vapor with minor contributions from methane and nitric oxide also. The spectrum that is shown in Figure 11a was obtained over the Sahara Desert. It manifests a pronounced residual ray or "reststrahlen" effect on the high wave number side of the atmospheric window between 1070 and 1250^{-1}. The spectrum from the more northern part of the Sahara near the Atlas mountains (Figure 11b) reveals distinctly different reststrahlen.

The spectrum from the moist area of the Niger Valley (Figure 11c) does not exhibit a residual ray effect at all; vegetation covers the ground and shields the minerals responsible for the effect, primarily silicon dioxide, from exposure. In this wave number range, plants as well as water are nearly black.

The spectra of the polar regions are quite different from the spectra of the tropical desert areas. The brightness temperature of the Greenland ice cap (Figure 12a) follows the 240 K blackbody temperature curve except for the 667 cm^{-1} CO_2 band. The lower brightness temperature in that range is an indication of lower atmospheric temperatures, except for the Q branch at 667 cm^{-1} which signals a reversal of the temperature profile toward a warmer stratosphere. The strong water vapor lines between 400 and 550 cm^{-1} appear in absorption. The ozone band near 1040 cm^{-1} registers very weakly not because of a lack of O_3 but because the weighted mean temperature of the layer is almost the same as the temperature of the surface. An Antarctic spectrum (Figure 12b) indicates a surface temperature of about 223 K and only small amounts of water vapor. In another Antarctic spectrum (Figure 12c), some atmospheric layers seem to be warmer than the surface which is very cold, about 205 K. Water vapor lines appear in emission, but ozone is not detectable because of a lack of temperature contrast between the ozone layer and the ground. In the coldest spectrum recorded on this orbit (Figure 12d), the whole atmosphere is warmer than the surface; carbon dioxide, water vapor, and ozone can be recognized as emission features.

The spectra in Figure 13 have been chosen to demonstrate the effect of partial cloudiness. All three spectra were recorded over tropical areas, Figure 13a over Micronesia, when the field of view was cloud free but there was possibly some haze present, and Figures 13b and 13c over the Ivory Coast when there were increasing amounts of cold clouds within the field of view of the instrument. In the nearly clear case (Figure 13a), the radiance of the atmospheric window follows a blackbody brightness of approximately 295 K, except for the 800 cm^{-1} range where a slight drop in the temperature may be noted. When a substantial part of the field-of-view is covered by cold clouds, a lower brightness temperature than the actual surface temperature, as well as a deviation from a blackbody function, is expected. The effect is apparent in Figure 13b and even more so in Figure 13c. The "cloud" emissivity cannot be ruled out as a possible contributor to the effect to a lesser degree.

In contrast to the characteristic behaviour of partial cloudiness, an essentially solid cloud deck more nearly follows the Planck function corresponding to the temperature near the cloud top (see Figure 14c). The other spectra in Figure 14 illustrate the variety in the appearance of the CO_2 band, which reflects the variety of temperature profiles that were encountered.

As it was pointed out previously, the wide spectral range covered, the radiometric quality, the precision, the spectral and spatial resolutions, the global coverage, and the availability of the spectra for a period of more than one year make these data a valuable and unique assembly of information

suitable for research in many areas of geophysical science. Some avenues of research will be explored in the papers that are to follow.

PLANNED INVESTIGATIONS

A number of research tasks are being pursued currently using calibrated spectra from IRIS-D. The results of these studies will be reported in subsequent papers in this series. The spectra provide an excellent source of data for many purposes including investigations of certain fundamental questions associated with radiative transfer in the terrestrial atmosphere. Work of this nature can be based on comparisons between measured spectra and spectra calculated by the line by line integration technique in combination with in situ atmospheric measurements. This approach will be followed in the second paper of the series.

In the third paper, techniques for obtaining vertical temperature profiles will be examined. Because data are obtained at relatively high spectral resolution from the entire 667 cm^{-1} CO_2 absorption band, it is possible to study the effects on the soundings of the number, location, and bandwidth of spectral intervals. The agreement of remote soundings with rawinsonde and rocketsonde data will be judged by statistical comparisons between ensembles of nearly simultaneous in situ and satellite measurements.

The large body of data acquired is well suited for a study of the statistical properties of the thermal emission spectrum of the earth and atmosphere. The fourth and fifth papers in the series will be devoted to this task.

Also, a correlation analysis of various portions of the spectrum will assist in the choice of optimum spectral intervals for vertical sounding. In addition, such correlations are expected to reveal certain physical interrelations among atmospheric levels. The study of mean and standard deviation spectra, along with characteristic pattern analyses, will be used to establish the total information content of the spectra. Information on certain physical parameters such as minor constituents and surface reststrahlen will be presented also.

Paper six will be concerned with the retrieval of the verticle distribution and total amount of minor atmospheric constituents such as water vapor, ozone, and possibly other gases. The global fields of temperature and ozone derived from the spectra will be examined in papers seven and eight. In subsequent papers, the effects of particulate matter on the spectra will be investigated, and possibly, seasonal effects will be presented.

ACKNOWLEDGMENT

We are grateful to Mr. L. R. Blaine, GSFC, for making laboratory measurements of the warm calibration source.

REFERENCES

Buettner, K. J. K., and C. D. Kern, The Determination of Infrared Emissivities of Terrestrial Surfaces, J. Geophys. Res., 70, 1329 (1965).

Conrath, B. J., R. A. Hanel, V. G. Kunde, and C. Prabhakara, The Infrared Interferometer Experiment on Nimbus 3, J. Geophys. Res., 75, 5831 (1970).

Ellis, P. J., G. Peckham, S. D. Smith, J. T. Houghton, C. G. Morgan, C. D. Rodgers and E. J. Williamson, First Results from the Selective Chopper Radiometer on Nimbus 4, Nature, 228, 139 (1970).

Hanel, R. A., and B. J. Conrath, Interferometer Experiment on Nimbus 3: Preliminary Results, Science, 165, 1258 (1969).

Hanel, R. A., B. Schlachman, F. D. Clark, C. H. Prokesh, J. B. Taylor, W. M. Wilson, and L. Chaney, The Nimbus 3 Michelson Interferometer, Appl. Opt., 9, 1767 (1970).

Hanel, R. A., B. Schlachman, D. Rodgers, and D. Vanous, The Nimbus 4 Michelson Interferometer, Appl. Opt., 10, 6, 1376 (1971).

Kaplan, L. D., Inference of Atmospheric Structure from Remote Radiation Measurements, J. Opt. Soc. Amer., 49, 1004, (1959).

King, J. I. F., The Radiative Heat Transfer of Planet Earth, in Scientific Uses of Earth Satellites, edited by J. A. Van Allen, University of Michigan Press, Ann Arbor (1956).

Moller, F., and E. Raschke, Problems of Meteorological Observations from Satellites, Space Sci. Rev., 9, 90 (1969).

Wark, D. Q., and D. T. Hilleary, Atmospheric Temperature: Successful Test of Remote Probing, Science, 165, 1256 (1969).

FIGURE CAPTIONS

Figure 1 – Central portion of a typical cold calibration interferogram. The abscissa is proportional to optical path difference. The envelope around the interferogram is used to detect and eliminate spikes such as the one in the figure.

Figure 2 – Geometry employed in the calculation of the net power reaching the detector.

Figure 3 – Emissivity of the on-board calibration source based on a laboratory measurement.

Figure 4 – Calculated instrument temperature as a function of wave number. Under ideal conditions, the calculated instrument temperature should agree with the temperature, measured by sensors located in the instrument, which is shown by the broken horizontal line.

Figure 5 – Factor employed in the calibration to correct for imbalance between cold and warm calibration ports.

Figure 6 – The factors Φ and ψ used to correct for effects due to variation in instrument temperature with orbital position. The time scale is measured relative to the time the satellite enters the earth's shadow. The dots indicate the standard deviations obtained in calculating the factors.

Figure 7 – Daily mean instrument responsivities for the dates shown. Virtually no change in the responsivity can be detected over the time interval considered here.

Figure 8 – Noise equivalent radiance as a function of wave number for the dates shown.

Figure 9 – Interferograms employed in the image motion test described in the text. Interferogram A was obtained when the field of view was filled with a cold cloud; interferogram B was obtained from a warm surface. Interferogram C is a combination of interferograms A and B and is used to simulate passage from a cold cloud to a warm surface during the time an interferogram is being recorded.

Figure 10 – Spectra employed in the image motion test described in the text. Spectra A, B, and C were obtained from interferograms A, B, and C in Figure 9. The spectrum labeled (A+B)/2 is calculated from the mean of interferograms A and B.

Figure 11 – Examples of spectra obtained over North Africa. Blackbody curves for selected temperatures are included for comparison. Variations in the surface emissivity are apparent in the 1100-1200 cm^{-1} region.

Figure 12 – Examples of polar spectra. The spectrum in Part (a) was obtained over Greenland; the spectra in Parts (b), (c), and (d) were obtained over Antarctica.

Figure 13 – Sample spectra illustrating effects of clouds in the window region of 800 to 1000 cm^{-1}. In this spectral region, a pronounced departure from a blackbody curve is noted in Parts (b) and (c) in contrast to the spectra shown in Figure 14, for example.

Figure 14 – Sample spectra illustrating the effects of different types of temperature profiles on the 667 cm^{-1} CO_2 band. The shape of the central portions of the band reflects the behavior of the temperature profile in the vicinity of the tropopause and in the stratosphere.

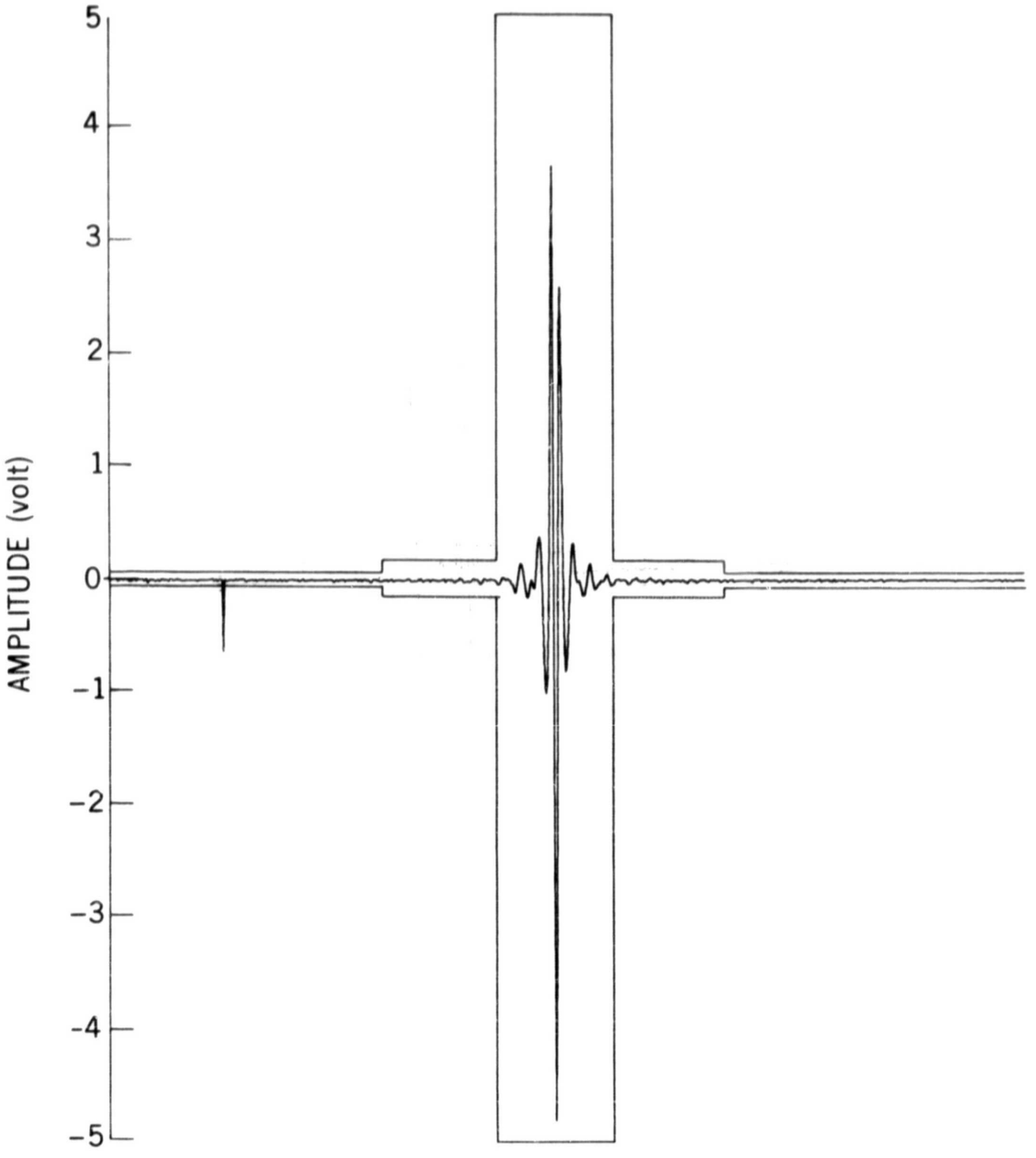

Figure 1 – Central portion of a typical cold calibration interferogram. The abscissa is proportional to optical path difference. The envelope around the interferogram is used to detect and eliminate spikes such as the one in the figure.

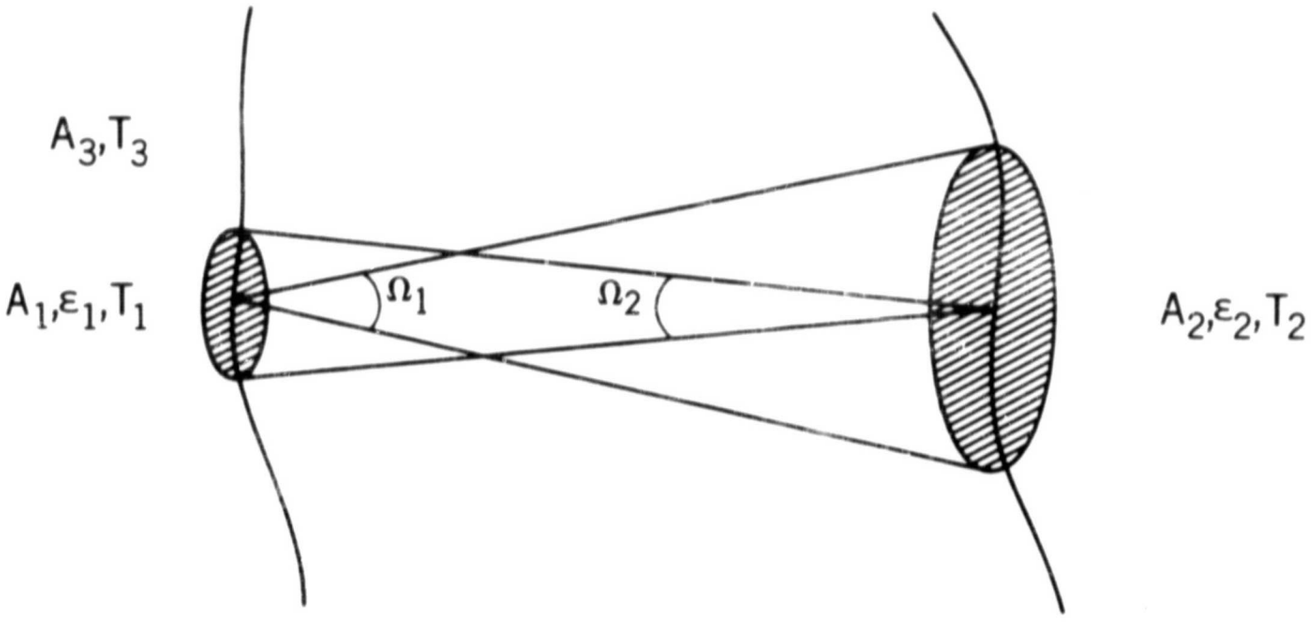

Figure 2 – Geometry employed in the calculation of the net power reaching the detector.

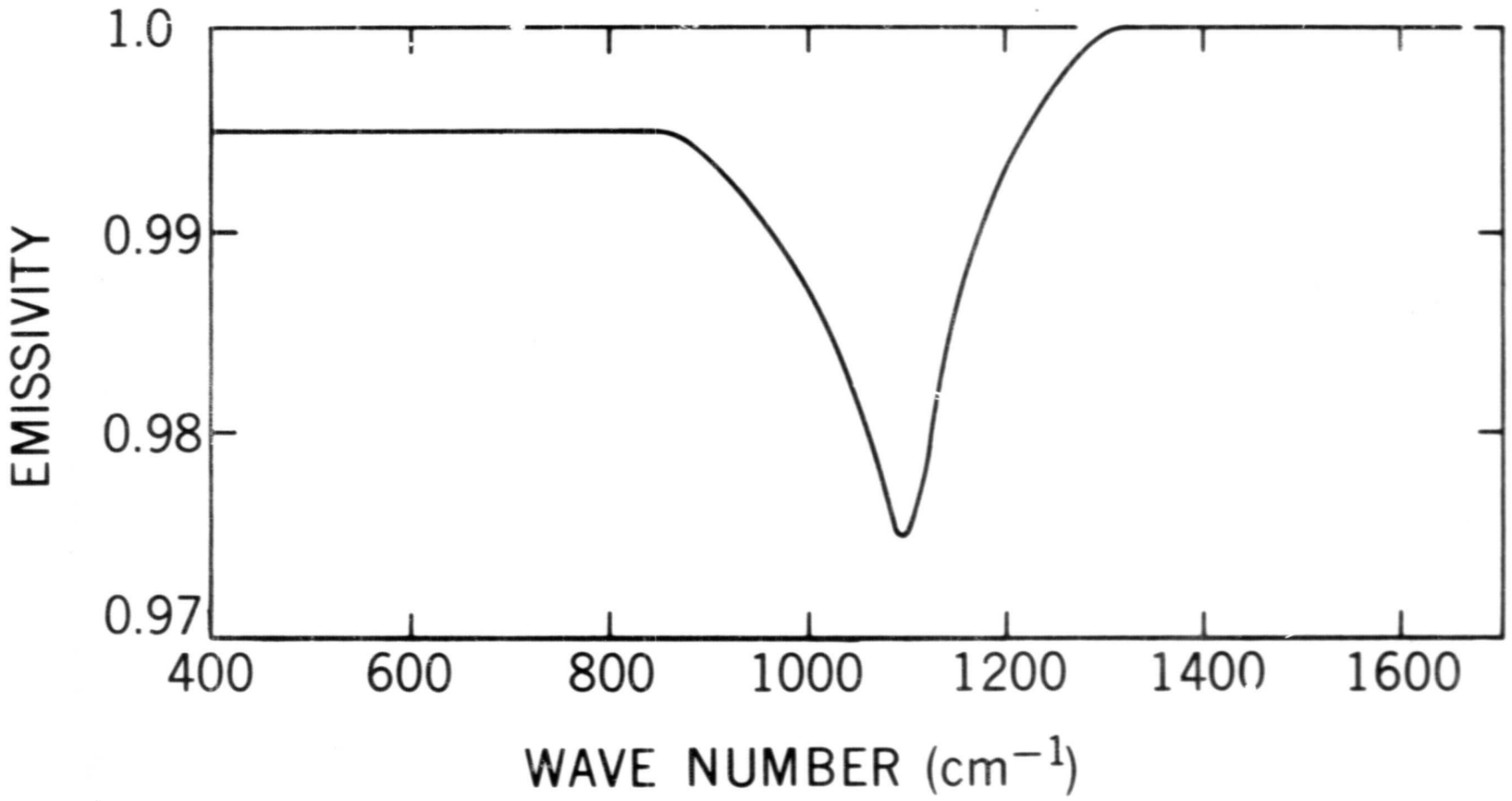

Figure 3 – Emissivity of the on-board calibration source based on a laboratory measurement.

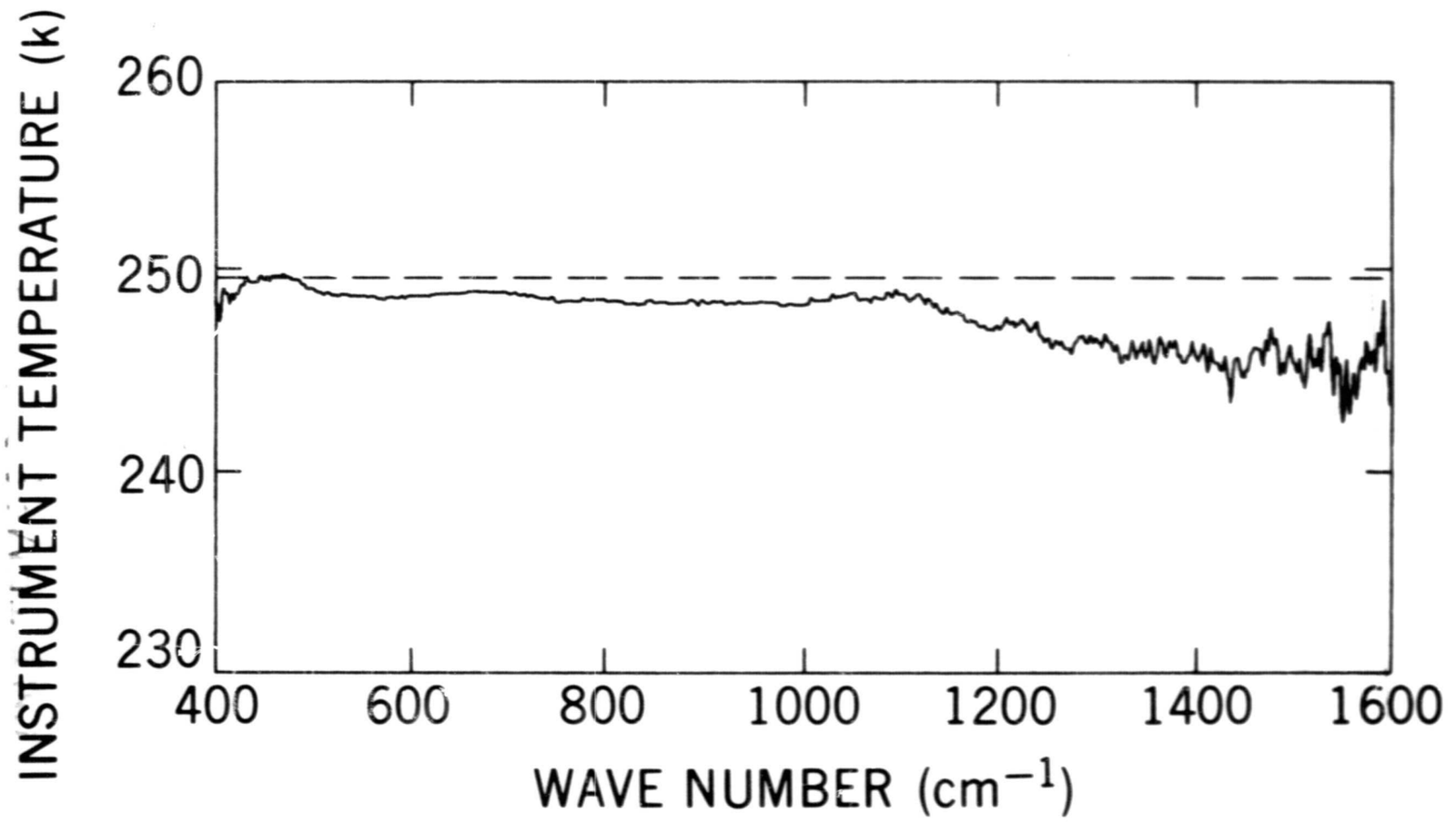

Figure 4 – Calculated instrument temperature as a function of wave number. Under ideal conditions, the calculated instrument temperature should agree with the temperature, measured by sensors located in the instrument, which is shown by the broken horizontal line.

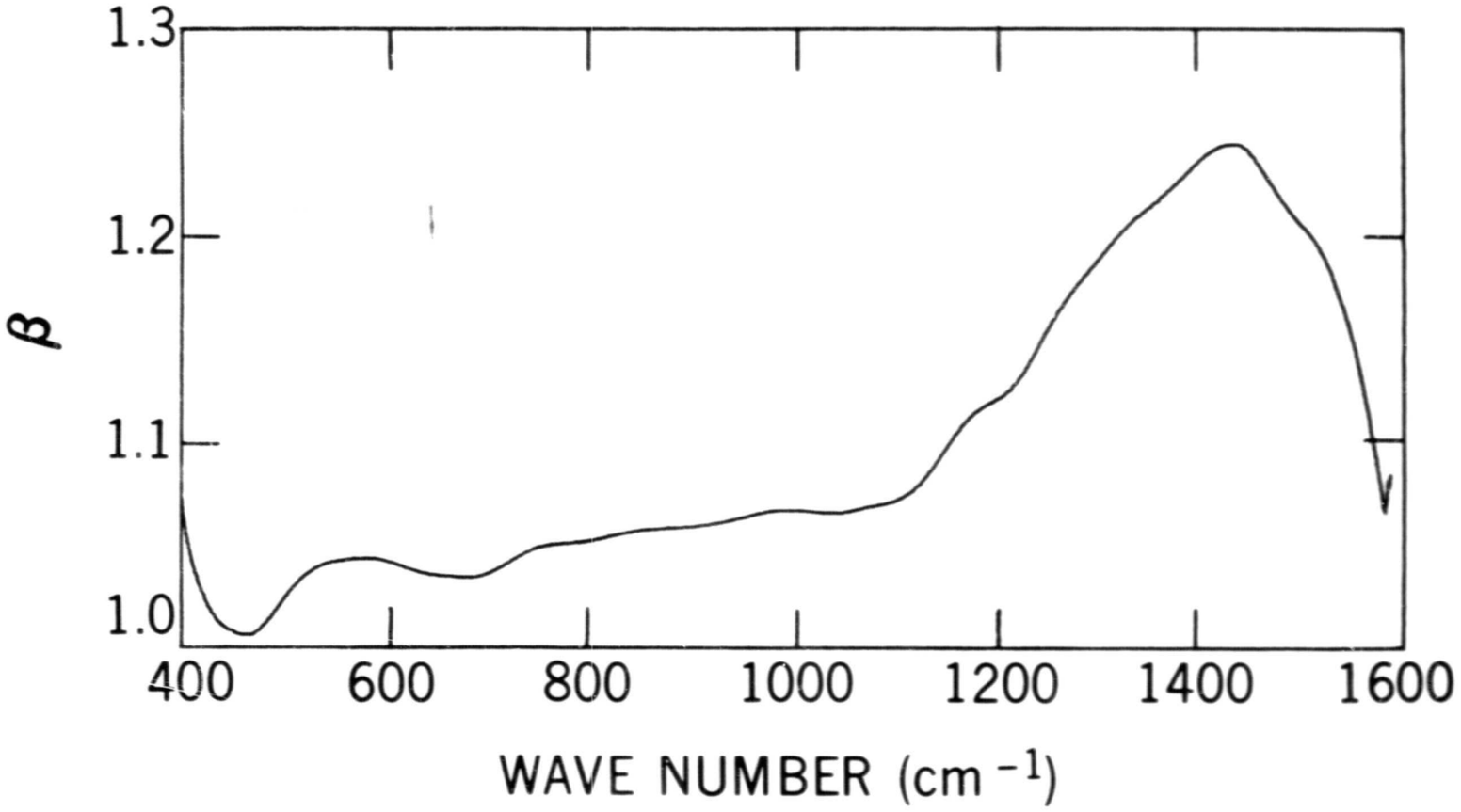

Figure 5 – Factor employed in the calibration to correct for imbalance between cold and warm calibration ports.

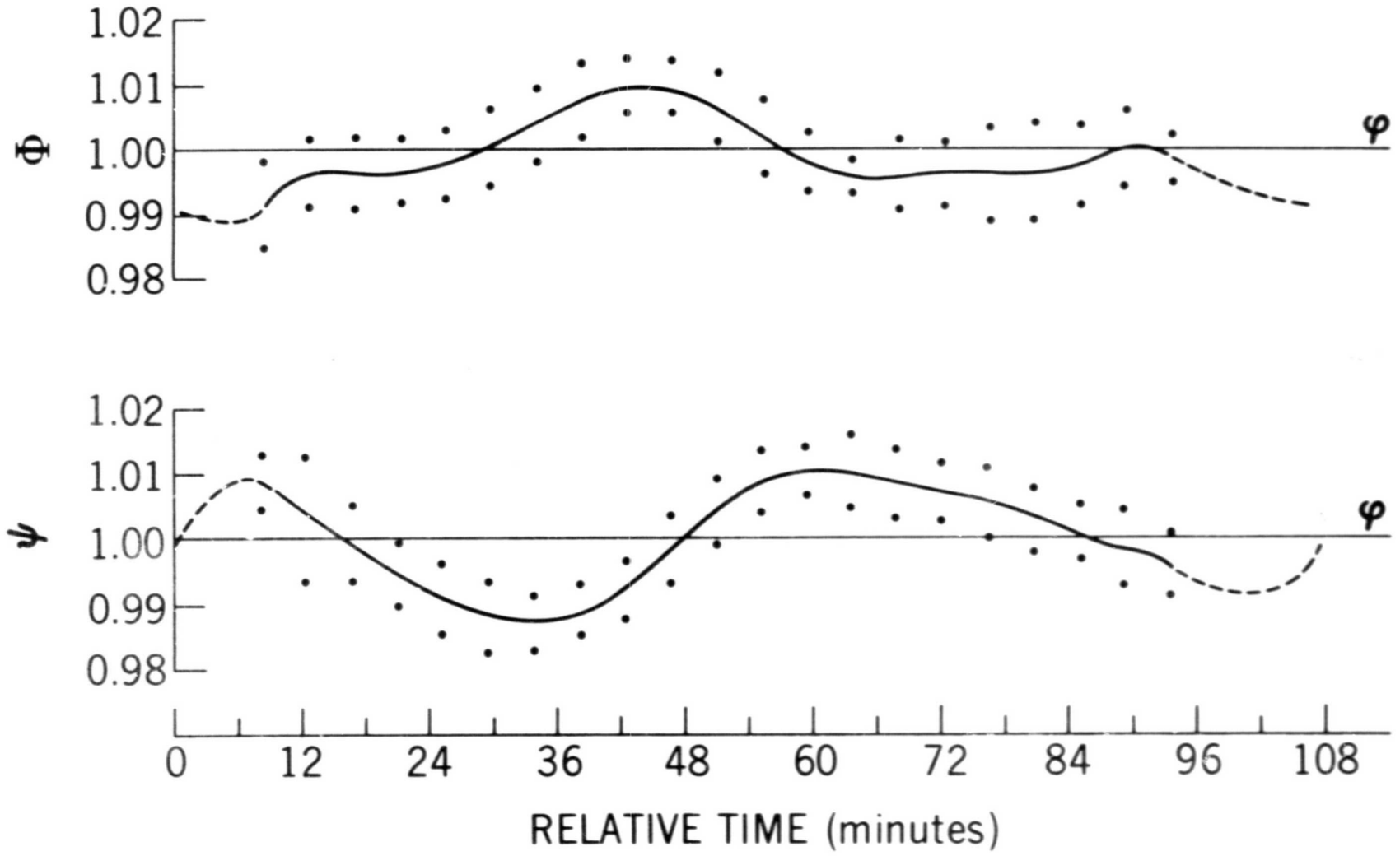

Figure 6 – The factors Φ and ψ used to correct for effects due to variation in instrument temperature with orbital position. The time scale is measured relative to the time the satellite enters the earth's shadow. The dots indicate the standard deviations obtained in calculating the factors.

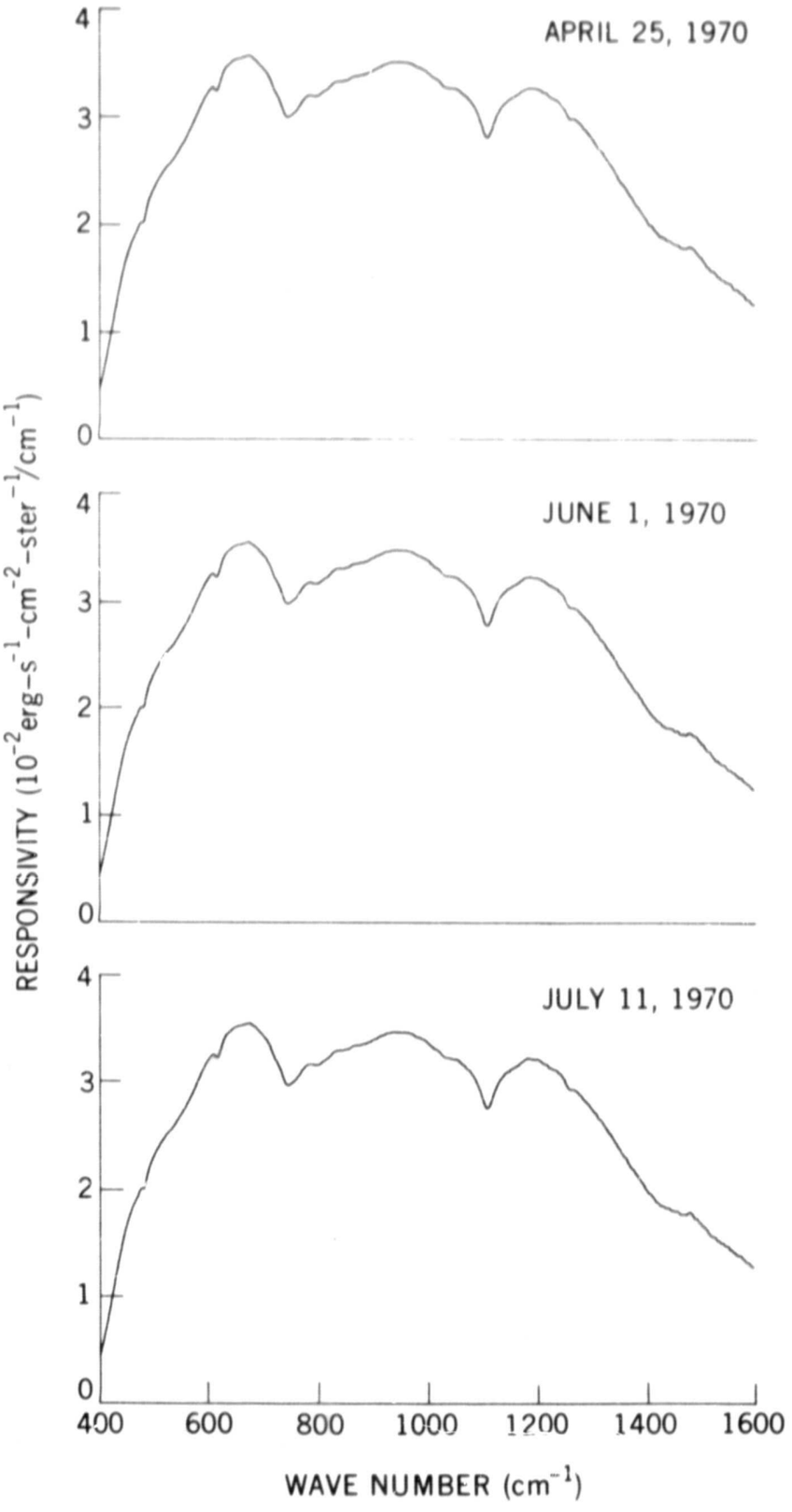

Figure 7 – Daily mean instrument responsivities for the dates shown. Virtually no change in the responsivity can be detected over the time interval considered here.

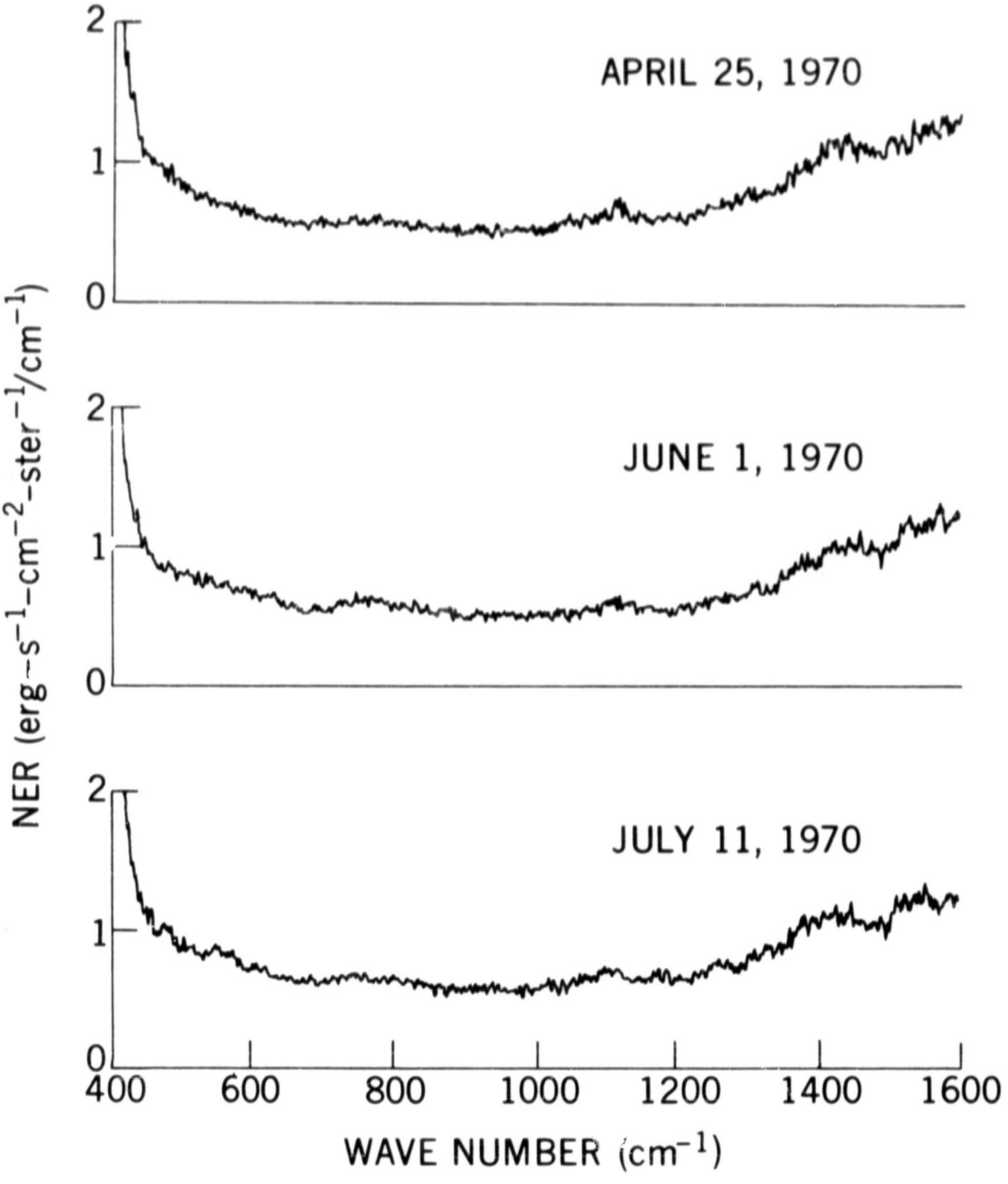

Figure 8 – Noise equivalent radiance as a function of wave number for the dates shown.

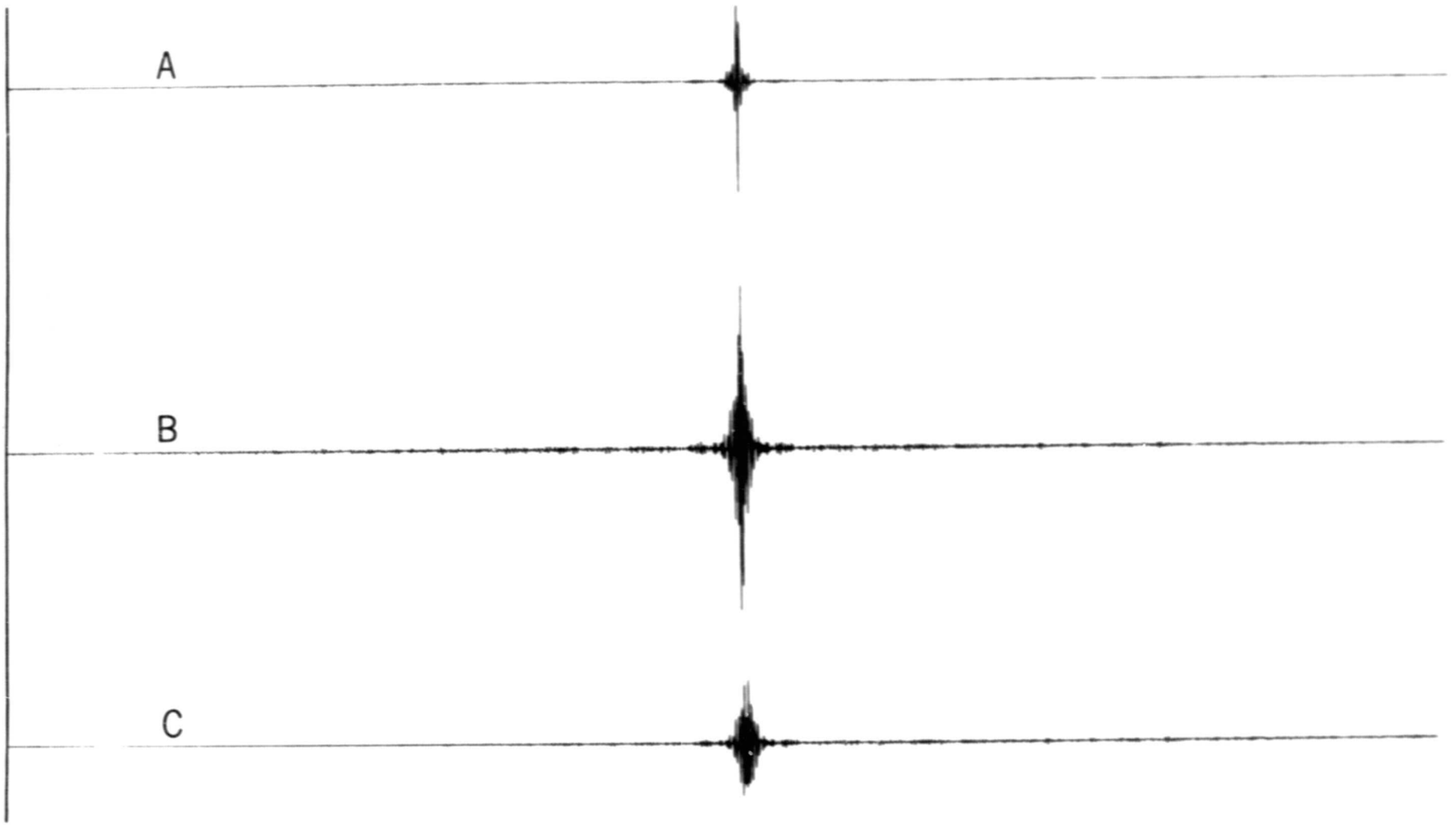

Figure 9 – Interferograms employed in the image motion test described in the text. Interferogram A was obtained when the field of view was filled with a cold cloud; interferogram B was obtained from a warm surface. Interferogram C is a combination of interferograms A and B and is used to simulate passage from a cold cloud to a warm surface during the time an interferogram is being recorded.

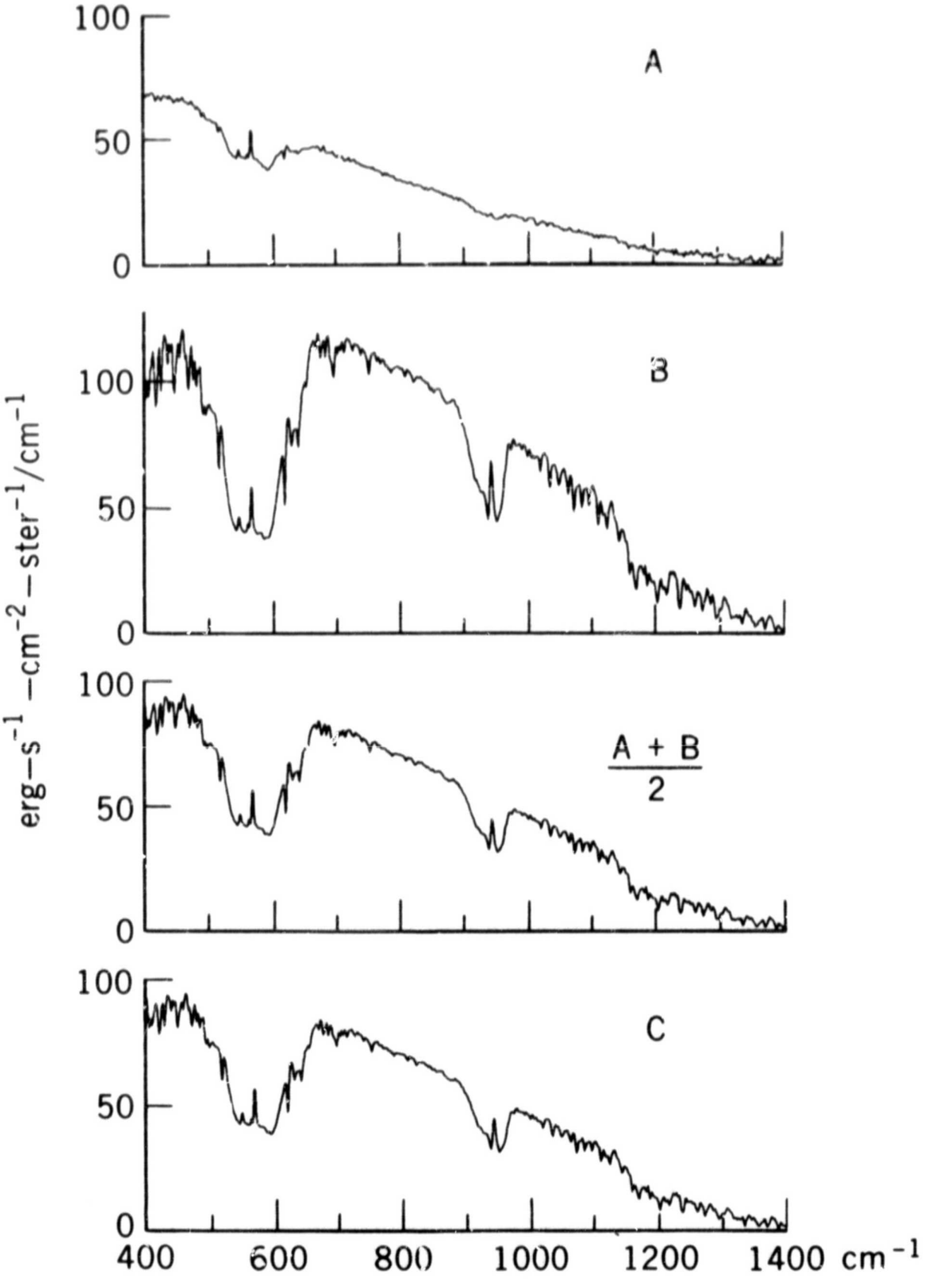

Figure 10 – Spectra employed in the image motion test described in the text. Spectra A, B, and C were obtained from interferograms A, B, and C in Figure 9. The spectrum labeled (A+B)/2 is calculated from the mean of interferograms A and B.

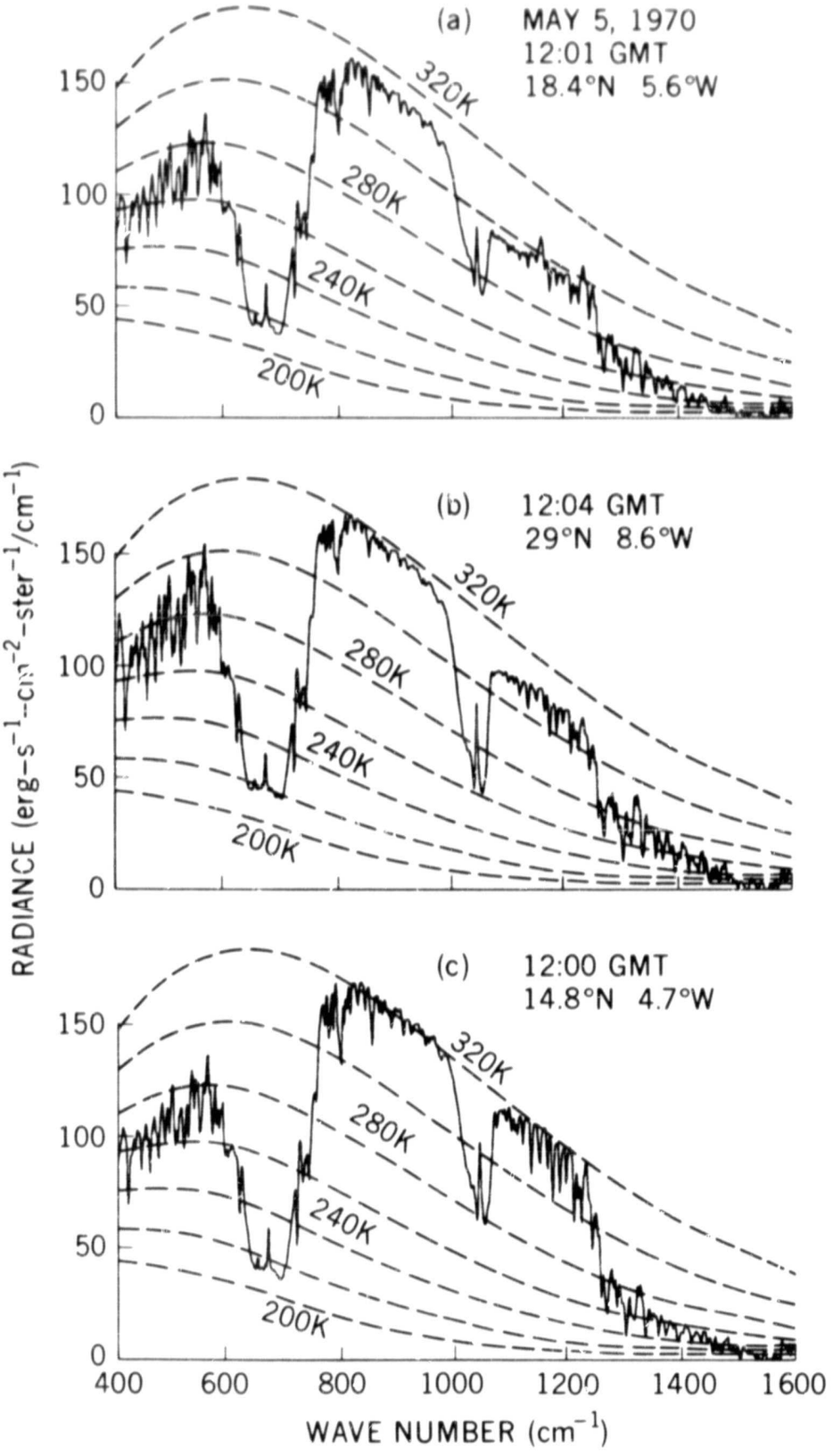

Figure 11 – Examples of spectra obtained over North Africa. Blackbody curves for selected temperatures are included for comparison. Variations in the surface emissivity are apparent in the 1100-1200 cm^{-1} region.

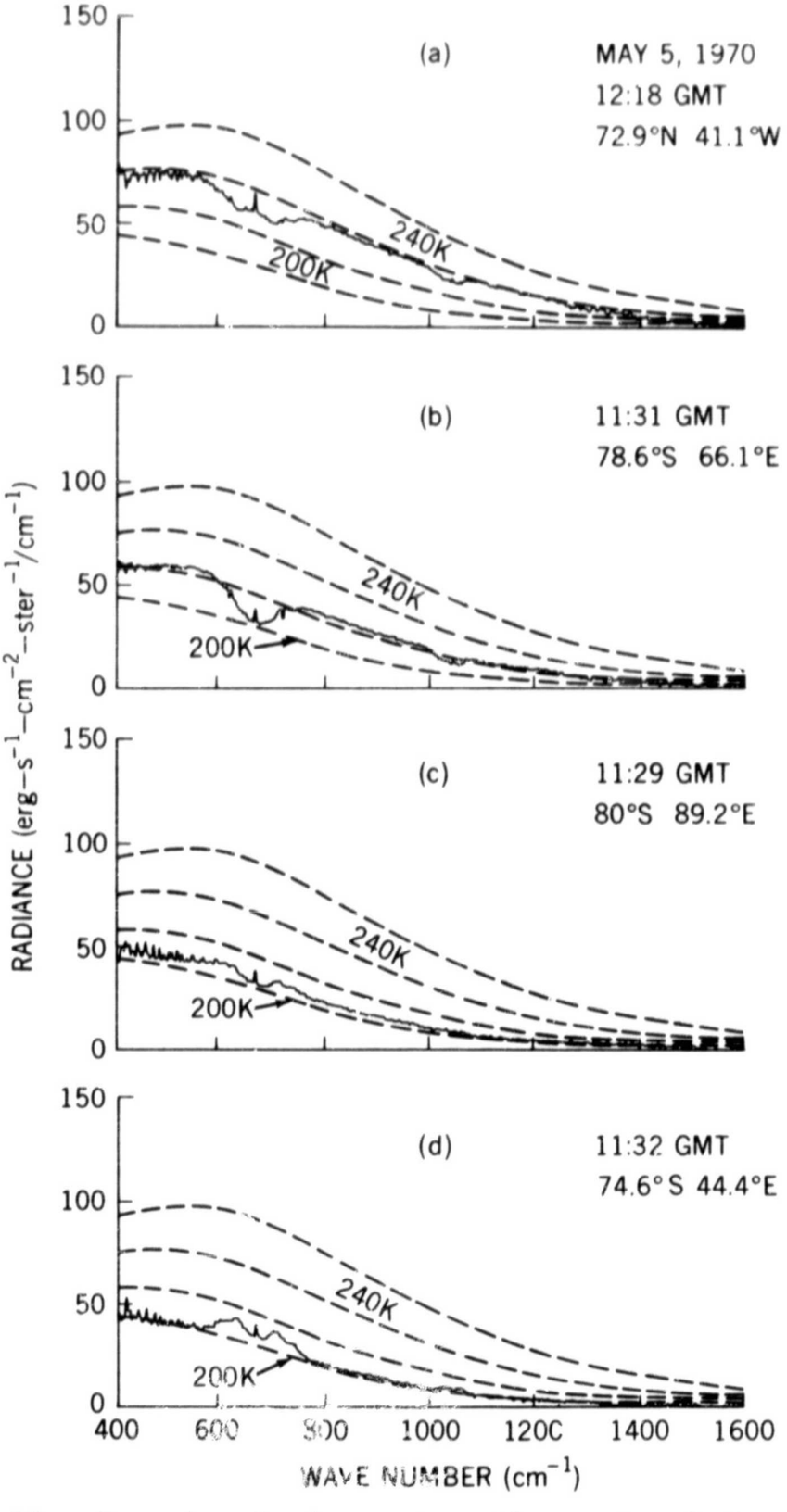

Figure 12 – Examples of polar spectra. The spectrum in Part (a) was obtained over Greenland; the spectra in Parts (b), (c), and (d) were obtained over Antarctica.

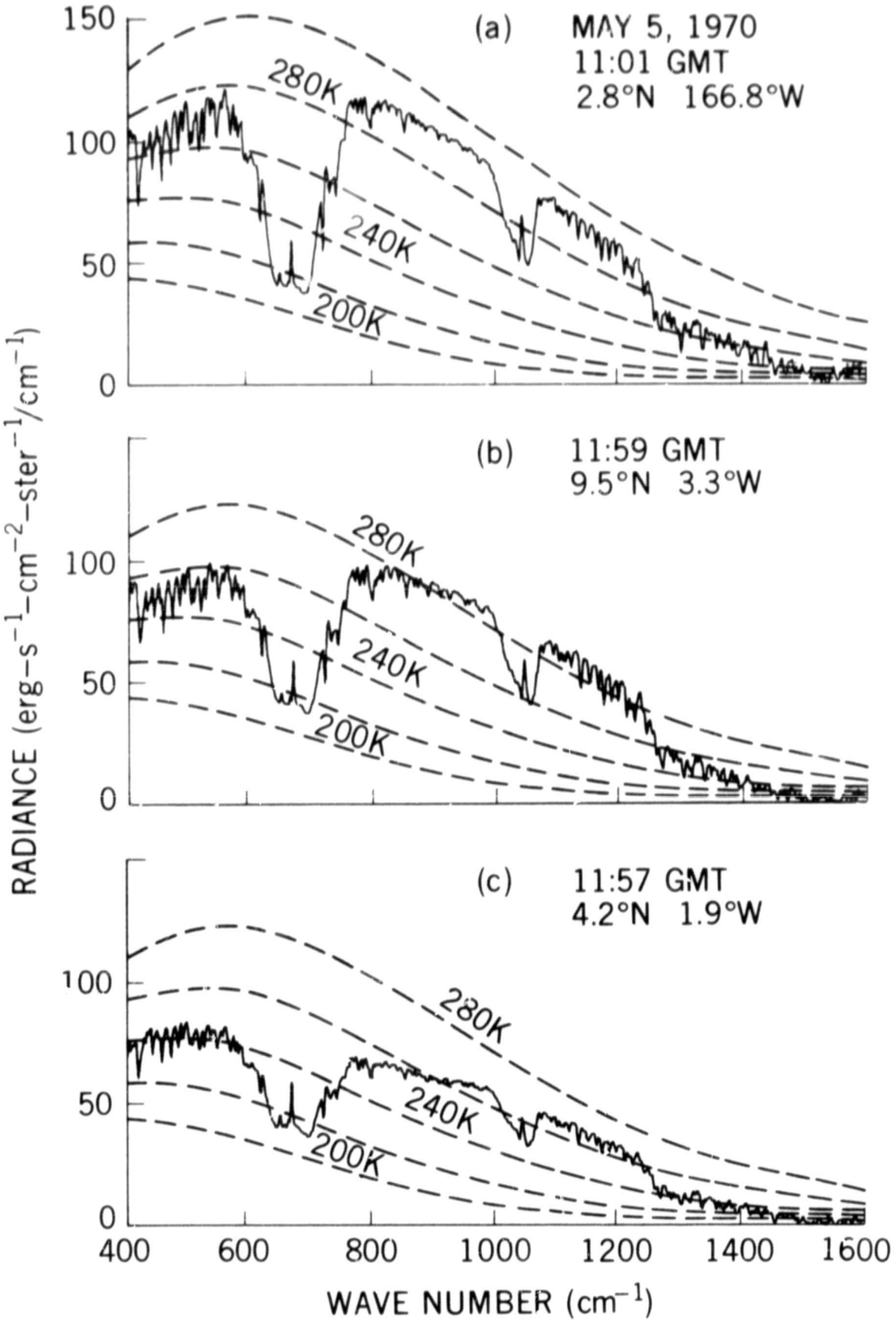

Figure 13 – Sample spectra illustrating effects of clouds in the window region of 800 to 1000 cm^{-1}. In this spectral region, a pronounced departure from a blackbody curve is noted in Parts (b) and (c) in contrast to the spectra shown in Figure 14, for example.

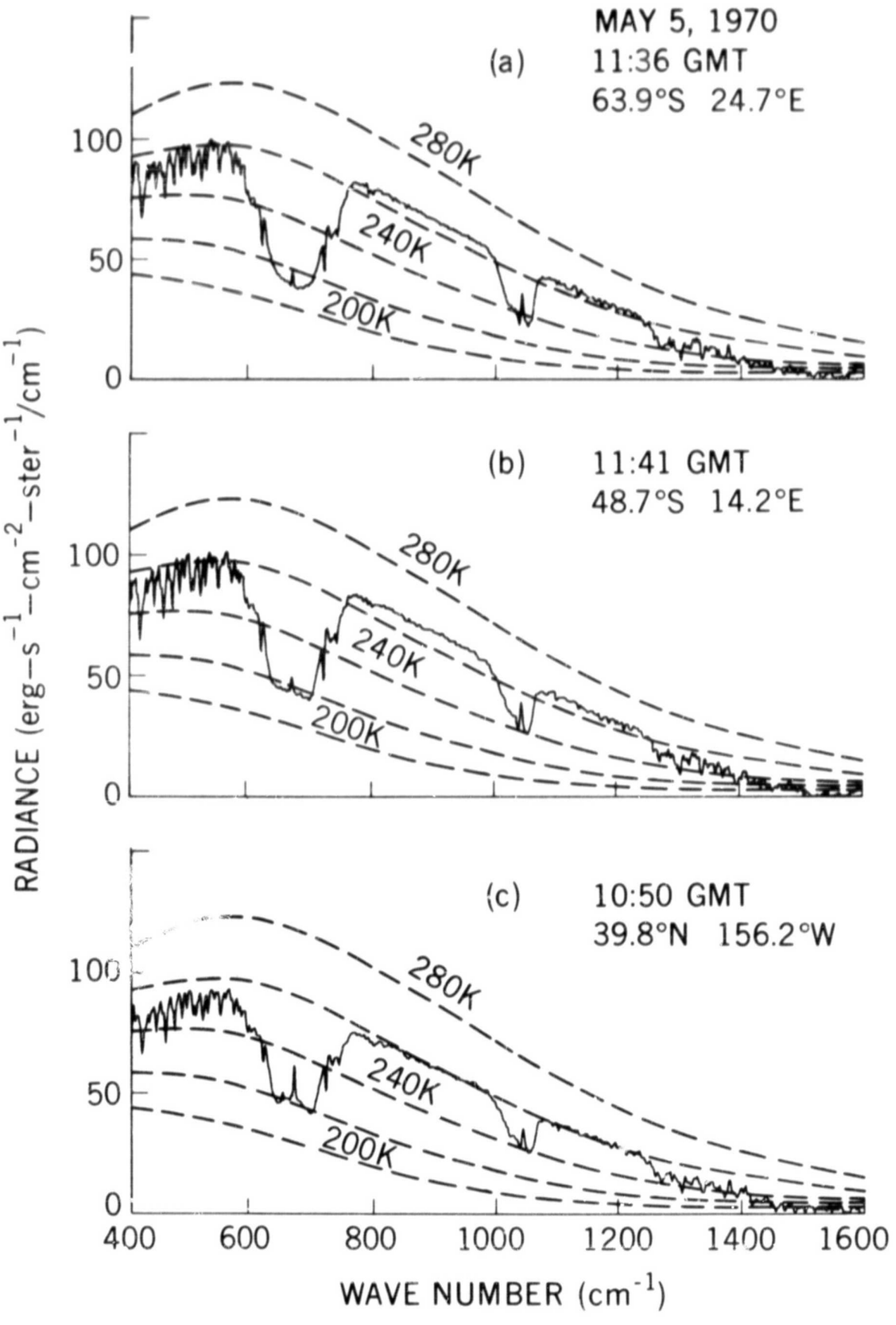

Figure 14 – Sample spectra illustrating the effects of different types of temperature profiles on the 667 cm^{-1} CO_2 band. The shape of the central portions of the band reflects the behavior of the temperature profile in the vicinity of the tropopause and in the stratosphere.